

REPORT DOCUMENTATION PAGE

*Form Approved
OMB No. 0704-0188*

The public reporting burden for this collection of information is estimated to average 1 hour per response, including the time for reviewing instructions, searching existing data sources, gathering and maintaining the data needed, and completing and reviewing the collection of information. Send comments regarding this burden estimate or any other aspect of this collection of information, including suggestions for reducing the burden, to Department of Defense, Washington Headquarters Services, Directorate for Information Operations and Reports (0704-0188), 1215 Jefferson Davis Highway, Suite 1204, Arlington, VA 22202-4302. Respondents should be aware that notwithstanding any other provision of law, no person shall be subject to any penalty for failing to comply with a collection of information if it does not display a currently valid OMB control number.

PLEASE DO NOT RETURN YOUR FORM TO THE ABOVE ADDRESS.

1. REPORT DATE (DD-MM-YYYY) 11/12/2007		2. REPORT TYPE Final Technical		3. DATES COVERED (From - To) 06/01/2003 - 08/31/2007	
4. TITLE AND SUBTITLE Towards Fieldable Rapid Bioagent Detection: Advanced Resonant Optical Waveguide and Biolayer Structures for Integrated Biosensing				5a. CONTRACT NUMBER	
				5b. GRANT NUMBER N00014-03-1-0815	
				5c. PROGRAM ELEMENT NUMBER	
6. AUTHOR(S) Hornak, Lawrence A. Korakakis, Dimitris Timperman, Aaron				5d. PROJECT NUMBER	
				5e. TASK NUMBER	
				5f. WORK UNIT NUMBER	
7. PERFORMING ORGANIZATION NAME(S) AND ADDRESS(ES) West Virginia University Research Corp on Behalf of West Virginia University Office of Sponsored Programs 886 Chestnut Ridge Road, Morgantown, WV 26506-6845				8. PERFORMING ORGANIZATION REPORT NUMBER NA	
9. SPONSORING/MONITORING AGENCY NAME(S) AND ADDRESS(ES) Dr. Laura Kienker Life Sciences Research Division, Code 341 Biosensors, Biomaterials, and Bio-inspired Systems ONR				10. SPONSOR/MONITOR'S ACRONYM(S)	
				11. SPONSOR/MONITOR'S REPORT NUMBER(S)	
12. DISTRIBUTION/AVAILABILITY STATEMENT No limitation on distribution					
13. SUPPLEMENTARY NOTES					
14. ABSTRACT This research project established the understanding necessary for the stacked planar affinity-regulated resonate optical waveguide (SPARROW) architecture to serve as a transducer device platform for rapid biomolecular detection. SPARROW structures have been grown with waveguide losses of less than 1 dB/cm. Thin biolayers of less than 10 nm were achieved and SAM attachment to polycrystalline surfaces studied. SPARROW transducer measurements were conducted using sucrose analyte solutions applied to the top waveguide surface via a PDMS microfluidic channel. For a flow channel and waveguide interaction width of 1200 microns, detection equivalent to a surface loading of from 10 to 1 pg/mm ² was achieved under different SPARROW surface conditions. Achievable detection was modeled and indicated a Limit of Detection (LODs) lower than 0.1 pg.mm ² for spore sized targets.					
15. SUBJECT TERMS biosensor, optical waveguide, SPARROW, SAM, anthrax					
16. SECURITY CLASSIFICATION OF:			17. LIMITATION OF ABSTRACT	18. NUMBER OF PAGES	19a. NAME OF RESPONSIBLE PERSON
a. REPORT	b. ABSTRACT	c. THIS PAGE			19b. TELEPHONE NUMBER (Include area code)
NA	NA	NA	None	22	

Project Title: Towards Fieldable Rapid Bioagent Detection: Advanced Resonant Optical Waveguide and Biolayer Structures for Integrated Biosensing

ONR Award No: N000140310815

Program: DEPSCoR

Total Award Period: June 1, 2003 - August 31, 2007

Technical PI/Contact:

Dr. Lawrence Hornak
West Virginia University
Lane Dept of Comp. Sci. and Electrical Engineering
Morgantown, WV
26506-6109
Phone: 304 293 0405 x2515
Fax: 304 293 8602
lah@csee.wvu.edu

Co-PIs: Dr. Aaron Timperman
Department of Chemistry, WVU
Dr. Dimitris Korakakis
Lane Dept of Comp. Sci. and Electrical Engineering, WVU

Table of Contents

Project Executive Summary	2
Technical Approach and Accomplishments	4
Impact on Research and Education Infrastructure	20
References	21

Project Executive Summary

Summary of Scientific and Technical Objectives

This research project established the understanding necessary for the stacked planar affinity-regulated resonant optical waveguide (SPARROW) architecture to serve as a transducer device platform for rapid biomolecular detection. The SPARROW is shown in Figure 1. The architecture features a simple planar structure enabling evanescent wave penetration depth and biolayer co-design for a specific target size. The SPARROW sensor consists of two planar, single mode aluminum oxide waveguides separated vertically by a lower refractive index silicon dioxide layer. The thicknesses and indices of all layers are designed to make the waveguides resonant, with matched modal indices in the presence of a water superstrate, allowing for the periodic exchange of the input power between the top and bottom waveguides. The width of the PDMS microchannel bonded to the top alumina waveguide determines the interaction length of light with the aqueous analyte. This width is typically designed for an odd number of coupling lengths so all power transfers to the opposite waveguide to which it was coupled. The extension of the

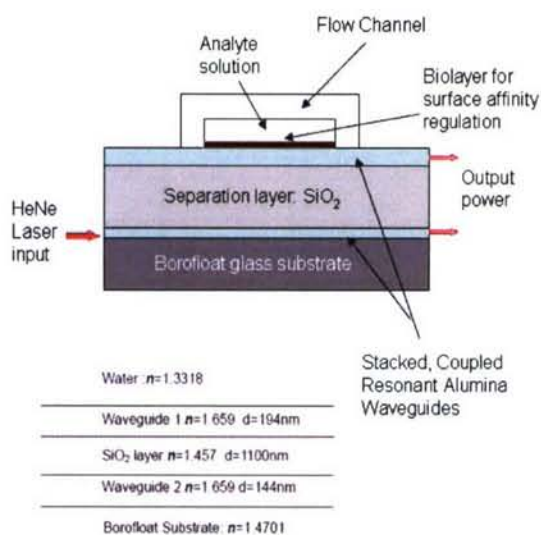


Fig. 1: The SPARROW device cross section and typical grown film stack characteristics.

evanescent field into the superstrate above the waveguides makes the tuning of the top waveguide sensitive to refractive index changes of the superstrate. Attachment of bio-agents to a specially designed biolayer above the waveguides changes the effective refractive index of the biolayer and detunes the top waveguide, changing the amount, periodicity, and rate of optical power transfer between the waveguides. This power change can be correlated to the refractive index of the bio-agent, allowing for detection of target molecules. The efforts of this research focused on the use of the SPARROW device for detection of biological targets on the scale of bacillus spores.

The research team's scientific and technical objectives were to 1.) Establish a process for SPARROW device growth and fabrication to achieve tuned resonant waveguides consistent with cointegration of microfluidic addressing and optical I/O, 2.) Establish attachment and coverage of the self-assembled monolayer (SAM) and selected recognition elements on as-grown alumina compatible with PDMS microfluidics, 3.) Model the SPARROW transduction behavior and its LOD, and 4.) Complete initial testing of the SPARROW transducer device.

Summary of Approach and Accomplishments

In our modeling and fabrication thrust, our goal was to achieve resonant waveguide stack growth and device fabrication control characterized by low optical loss and agreement between optically modeled and experimentally measured waveguide propagation constants. Our approach has been to understand and stabilize the characteristics of grown alumina and silicon dioxide films as a prerequisite to multilayer waveguide stack growth. This understanding has been achieved by a systematic study of resulting film physical and optical characteristics under specific growth conditions. This approach has yielded a process for low-loss SPARROW growth and co-integration of PDMS microfluidic addressing. Alumina waveguide stacks on borofloat substrates with silicon dioxide spacer layer have been grown with waveguide losses of less than 1 dB/cm. Transducer measurements were conducted using sucrose analyte solutions applied to the SPARROW surface via a PDMS microfluidic channel. For a flow channel and waveguide interaction width of 1200 μm , detection equivalent to a surface loading of from 10 pg/mm^2 to 1 pg/mm^2 was achieved under different SPARROW surface conditions.

The biolayer thrust focused on design and implementation of a thin homogenous layer that minimizes non-specific binding to the uppermost waveguide of the SPARROW device exposed to the analyte while using selective molecular recognition for target acquisition. Maximum sensitivity is achieved when the targets occupy the maximum space in the sensing volume which penetrates 50 nm into the analyte region, the distance of the top waveguide evanescent field. As a result, for the current focus on bacillus spore detection, the biolayer must be as thin as possible, preferably 10 nm or less. Our approach utilizes: self-assembled monolayers (SAMs) to provide a homogenous surface coating with minimal defects, terminal polyethylene glycol (PEG) tails to minimize non-specific protein adsorption, and a signaling peptide that selectively binds to a receptor on the target surface. Ideally, the SAM monolayer would be very stable, but could be easily removed and regenerated after the exposure to the sample. Therefore, the formation and stability of the various SAM monolayers were studied initially. When it was determined that SAMs formed from monomers with carboxylic acid head groups were not stable enough in water, the use of monomers with alternate head groups was explored. Fundamental studies characterized the desorption of SAMs from various monomers in water. A microfluidic channel was incorporated into the system to provide reproducible conditions for both reagent and target delivery, while minimizing the volume and mass of sample required. The binding and removal of target simulants were studied as a function of linear flow rate through the channel.

Bridging both waveguide and biolayer efforts, we modeled the LOD for this device class. We estimated the LOD for micron scale bacillus spore targets at small surface loadings by considering both the resonant coupling and the optical scattering due to the random spatial distribution of targets bound to the biolayer. It was determined that LODs of from 10 to 0.1 pg/mm^2 should be readily achievable with reasonable optical detector dynamic range, and even lower LODs may be practical with better optical detection and reduced

noise designs (e.g. differential devices using an optical reference path). This LOD estimation approach can be broadly extended to other device geometries relying on resonant waveguide detuning arising from selective biotarget surface binding. We successfully established an analytic model incorporating both physical mechanisms and evaluated it numerically for a typical biosensor waveguide stack.

We have successfully achieved the four main research objectives. However our fourth objective of transducer evaluation, while successful with the detectivity determined and consistent with models, was conducted only with sucrose solutions. The transducer has yet to be evaluated in combination with the biolayer. This work is ongoing. The research has succeeded in establishing an analytical and experimental understanding of the interdependence of biolayer and coupled resonant optical waveguide design necessary to quantify intrinsic limits of detection (LOD), optimize realizable extrinsic performance, and extend this important new class of devices to smaller targets in future work.

Technical Approach and Accomplishments

In this section we provide detailed discussion of the technical approaches and accomplishments of the program. This discussion is broken down into the following program elements: waveguide stack growth and characterization, transducer evaluation, biolayer growth and attachment, and LOD analysis.

Waveguide Stack Growth and Characterization

The use of ion beam assisted deposition (IBAD) electron beam evaporation has been investigated and used to produce low loss alumina waveguides and reduced strain silicon dioxide buffer layers for use in the SPARROW biosensor. It has been established in literature that the position of the Si-O in-phase stretch absorbance peak located around 1078 cm^{-1} is sensitive to strain in the SiO_2 film[1]. Our initial experiments studied the effects of the presence of water on e-beam deposited SiO_2 films and allowed us to arrive at the significant conclusion that the presence of water accelerates the strain relief seen by these films[2]. This is important in regards to the SPARROW biosensor, as it is designed to be used in a variety of atmospheres. With the introduction of IBAD deposition techniques, our group has determined that IBAD allows for as-deposited SiO_2 films with strain that approaches the value seen in fully relaxed SiO_2 films, as determined using Fourier Transform Infrared (FTIR) spectroscopy measurements and again tracing the position of the Si-O in-phase stretch absorbance peak. Reactive, IBAD SiO_2 depositions performed by evaporating Si source material in the ion source's oxygen atmosphere exhibited Si-O absorbance peak locations near the nominal value of 1078 cm^{-1} for fully relaxed SiO_2 films[3], whereas non-IBAD depositions resulted in Si-O peak locations at lower wavenumbers, indicative of higher strain. These results can be seen in Table 1. Thus, using IBAD reactive depositions, no absorption of water or aging must occur to have e-beam deposited SiO_2 films at a fully relaxed state of minimal strain. These films

have been observed over time, and no change in peak position was found, indicative of the stability of reactively deposited, IBAD SiO₂ depositions and their minimal water absorbance. Our group has found that reactive SiO₂ depositions also allow for a more reproducible deposition flux cloud due to the Si evaporation material forming a liquid phase during evaporation. This reproducible flux cloud allows for more reproducible film thicknesses, indices of refraction, and Si-O in-phase stretching peak locations, as compared to SiO₂ depositions from SiO₂ dielectric source material in a non-IBAD environment, as seen in Table I.

TABLE I : Thickness, index of refraction, and Si-O absorbance peak location for five samples in group 1 (deposited without ion source) and group 2 (reactively deposited with ion source).

Sample #	Group 1 Thick.	Group 1 Index	Group 1 Si-O Peak	Group 2 Thick.	Group 2 Index	Group 2 Si-O Peak
1	1079.2	1.4691	1076.8	1104.3	1.4753	1078.1
2	1138.3	1.4653	1075.7	1105.9	1.4745	1077.9
3	1067.7	1.4726	1075.9	1096.1	1.4762	1078.9
4	1084.4	1.4771	1076.1	1105.1	1.4755	1078.8
5	1109.6	1.4710	1073.4	1105.6	1.4744	1078.0
Mean	1095.4	1.4710	1075.6	1103.4	1.4753	1078.3
Std. Dev	28.3000	4.4000e-3	1.3000	4.1255	7.4600e-4	0.4722

In general, dielectric thin films from electron-beam evaporation with densities similar to that of the bulk material can be difficult to obtain due to the porosity and poor stoichiometry often seen in PVD deposited films[4]. It has been reported in literature that electron-beam deposition is in the form of columns, separated by low-density void regions, due to the low surface mobility of evaporated atoms and molecules[5]. The columnar thin film is of lower density than bulk material and unstable in air due to the relative humidity and the voids' tendency to fill with water[6]. The use of an ion beam to bombard the surface with energetic ions as the film is depositing has been reported to disrupt columnar deposition and increase film density towards that of the bulk material, due to the depositing molecules' increased energy and subsequently increased mobility on the substrate surface. The use of IBAD was thus applied for the deposition of low loss alumina waveguides, as the higher material density and decreased porosity should allow for the elimination of light scattering centers and subsequently lower losses.

When testing for light guiding properties using prism coupling methods, alumina films deposited without the ion beam assistance had little or no light guiding abilities. Conversely, all films deposited using ion beam assistance had light guiding ability that varied according to the ion beam parameters used for deposition. The dependence of propagation loss on ion source drive current is shown in Figure 2 and the dependence of propagation loss on oxygen flow rate is shown in Figure 3. These losses were calculated using a waveguide approach in which a right-angled gadolinium gallium garnet (GGG) glass prism of index 1.965 at 633 nm is used to couple light from a HeNe laser of wavelength 633 nm into the waveguides[7]. The waveguide streak was imaged using a

CCD camera and the losses calculated by processing the image of the light scattered from the surface of the film[8].

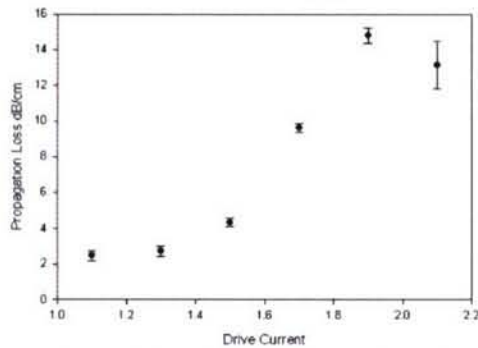


Fig. 2: Optical propagation loss for IBAD deposited alumina films as a function of ion source drive current[9].

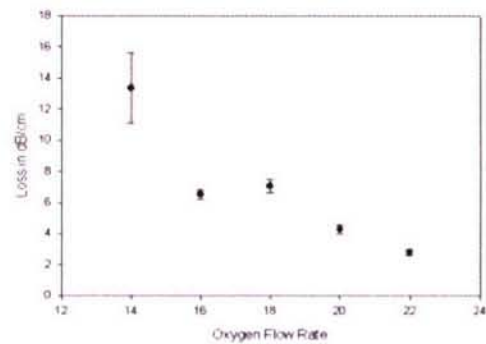


Fig. 3: Optical propagation loss for IBAD deposited alumina films as a function of oxygen flow rate[9].

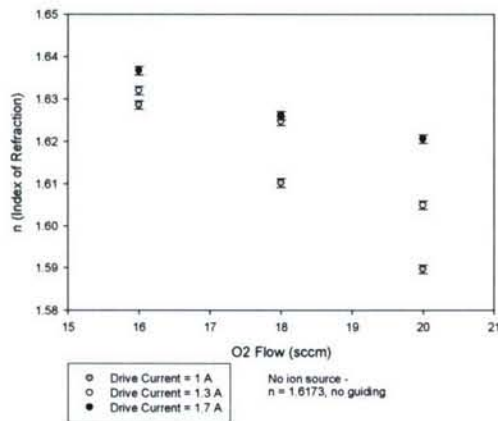


Fig 4: Dependence of Al₂O₃ index of refraction on oxygen gas flow rate and ion source drive current for alumina source material deposited under ion beam bombardment.

Another important aspect of the use of IBAD for alumina waveguide depositions is its ability to allow for the engineering of index of refraction. The tuning of the SPARROW biosensor is sensitive to very small changes in both thickness and index, so being able to accurately control the index of refraction is important in meeting the fabrication requirements for a tuned resonant structure. Additionally, being able to vary the refractive index allows for more flexibility when designing the parameters for the resonant structure. Figure 4 illustrates our use of IBAD to engineer the alumina films' indices of refraction by changing the ion source parameters O₂ flow rate and drive current.

The need for a strong optical signal at the terminal light read out positions despite input coupling loss, scattering loss, and other losses associated with the biosensor architecture is apparent. While IBAD is used in the waveguide deposition process to promote lower losses through the densification of films and elimination of porous scattering centers¹⁰, the losses for as-deposited films can still be prohibitive for biosensor operation. To further address this issue, our group has introduced the use of low temperature annealing for lowering losses in the alumina waveguides. Results indicate that annealing in the temperature range of 200° - 600° Celsius in air for short periods of time (2 - 10 minutes) improves waveguide propagation losses, reducing them to less than 1 dB/cm, as illustrated in Figure 5. The annealing is believed to be providing the energy needed to cause a change to the micro-crystalline structure of the alumina films, which could effectively grow or merge crystal grain

boundaries present and reduce the light scattering at these grain boundaries. Work is currently being done to further investigate this phenomenon.

The described studies provided the low loss coupled waveguide stacks which are the foundation for the SPARROW device.

SPARROW Transducer Fluidic Addressing and Transducer Evaluation

PDMS (Poly-dimethylsiloxane) microfluidic channels were fabricated and bonded to the stack waveguide structure to carry a constant analyte flow over the top waveguide and to introduce the SAM biolayer to the waveguide structure. A glass top PDMS channel was constructed which was found to be robust and prevent the collapse of the PDMS walls. To fabricate the PDMS channels, an SU-8 channel pattern was fabricated on a silicon substrate using standard photolithographic techniques and used as the master for creating the channel chips. The PDMS mixture was made using a 10:1 ratio of pre-polymer:curing agent and poured over the SU-8 master. The glass chips were cleaned in acetone for 30 minutes, dried in an oven for 10 minutes, and aligned over the SU-8 channel pattern. The wafer was heated in an oven for 1 hour at 120°C while aligning the chips periodically to assure the proper positioning of inlet and outlet holes over the channel pattern and then heated overnight. The PDMS chip was removed from the silicon wafer, and the input and output holes were drilled in the PDMS layer. The PDMS chip was cleaned in iso-propanol for 1 minute and dried in the oven for 10 minutes. The alumina waveguides were also cleaned for any polar or non-polar molecules present on the surface using toluene, acetone, hexane, toluene, and acetone for 5 – 10 minutes each in an ultrasonic bath. The waveguides were dried in the oven at 100°C for 20 minutes to remove any remaining moisture. Both the PDMS and waveguide surfaces were oxidized in an oxygen plasma chamber for 90 seconds. The PDMS chip was placed in DI water for 10 minutes and then dried in argon gas to form hydroxyl groups on the surface. The fabricated PDMS channel was placed on the alumina waveguide and heated in an oven for 12 hours at 120°C. Capillary tubes were inserted for inlet and outlet fluid flow. Key steps of the PDMS channel fabrication process are illustrated in Figures 6 and 7.

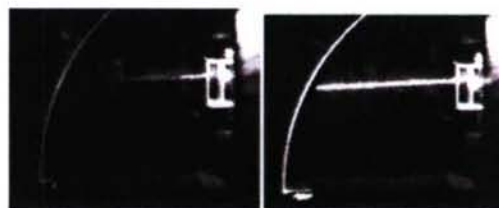


Fig 5: Waveguide images from a stacked, resonant waveguide structure before annealing (left) and after annealing (right), with reduction of propagation losses from approximately 3.0 dB/cm to 0.80 dB/cm.

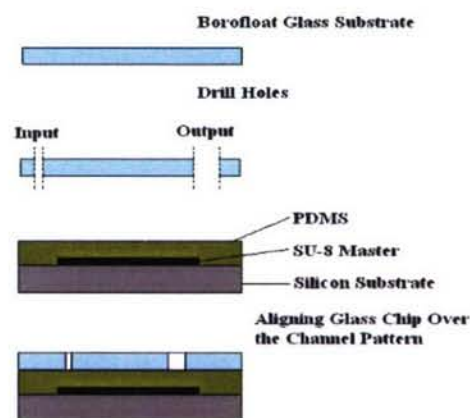


Fig 6: Fabrication of a glass top PDMS microchannel.

Prism coupling technology is used to observe the transduction mechanism of the SPARROW biosensor. The sample with attached PDMS channel is mounted in the prism coupler, and a HeNe laser operating at 632.8 nm is used to couple light into the waveguides. The prism coupler enables coupling of light into a single waveguide mode, allowing us to selectively couple light into either the top or bottom waveguide. After propagating through the sample interaction region, the light is coupled out of the top waveguide, allowing us to image the light in only the bottom waveguide using a CCD camera. Different exposure times are used, and images with pixels that are not saturated are selected for evaluation. The images are subjected to digital filtering to reduce image noise, and a dark image is taken and subtracted from the original image to reduce the effect of dark current. Initial sensor transducer results were obtained by flowing sucrose solutions of different concentrations through the sample flow channel and observing the bottom waveguide response. By comparing the pixel intensity present in the bottom waveguide when flowing sucrose solutions of different concentrations through the channel, the transduction performance of the SPARROW biosensor can be observed. The overall experimental setup and bonded PDMS channel are shown in Figure 8.

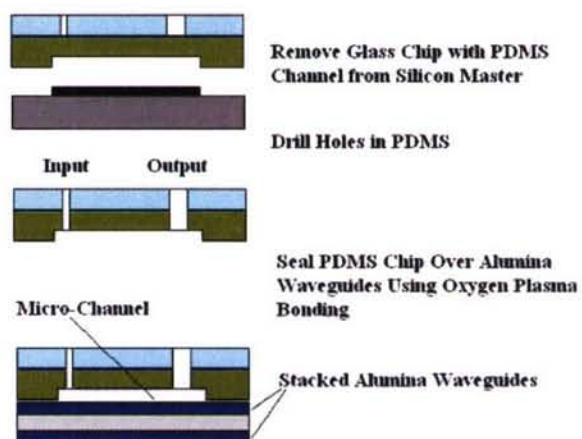


Fig 7: Alignment of PDMS channel over alumina waveguides.

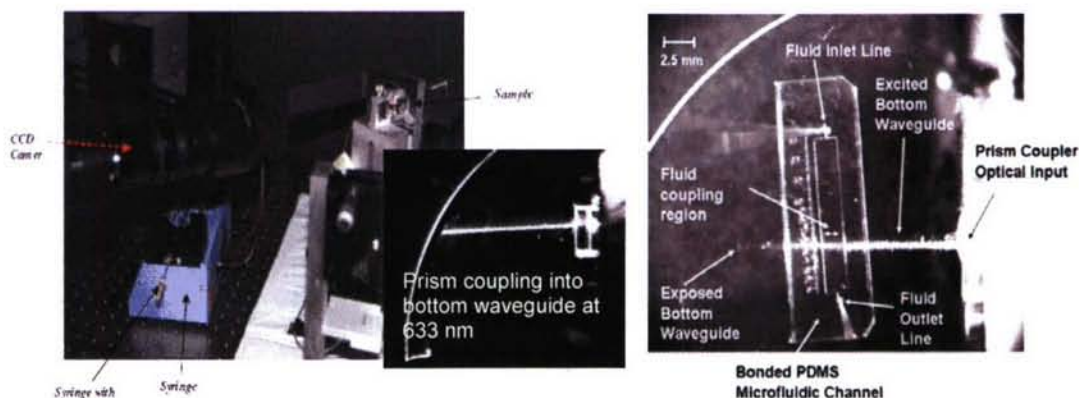


Fig 8: Prism coupler waveguide setup (right), coupled bottom waveguide in designed stack (center), SPARROW device under test with PDMS microfluidic analyte introduction to sensor top waveguide surface (right).

Transducer performance results for sucrose solutions are shown in Figure 9. Values of surface loading were obtained by determining the grams of sucrose for a given % W/V solution within a volume one optical penetration depth from the top alumina waveguide surface over 1 mm² of its area. This initial data shows a strong dependence on initial surface state resulting in a large optical intensity change with initial transition from DI water to sucrose solution analyte. This large transition is characteristic of a surface without sucrose attachment to the surface. We are currently implementing a NaCl – DI rinse protocol between different sucrose solutions in order to overcome charging effects that are believed to result in sucrose fouling of the alumina surface. Setting aside the initial transition from DI to sucrose solution, the transducer is readily able to detect changes of on the order 10 pg/mm², even in the presence of surface fouling. Assuming the initial transition in Figure 8 is more indicative of the unfouled surface that would be obtained with the biolayer that minimizes nonspecific binding discussed below, detection in the 1.0 pg/mm² range is readily achievable with no further improvement in optical detection. Improvement in optical detection sensitivity, coupled with dual optical path device architectures that enable differential optical detection may enable further performance improvements beyond 0.1 pg/mm². This would be a fruitful avenue for future work, however the transducer performance of the basic SPARROW device studied meets the objectives of the current project not only in desired surface loading detection range, but also in the area of device complexity and ultimate cost. This characteristic may be sacrificed with a negative impact on fieldability if a more complex architecture is employed.

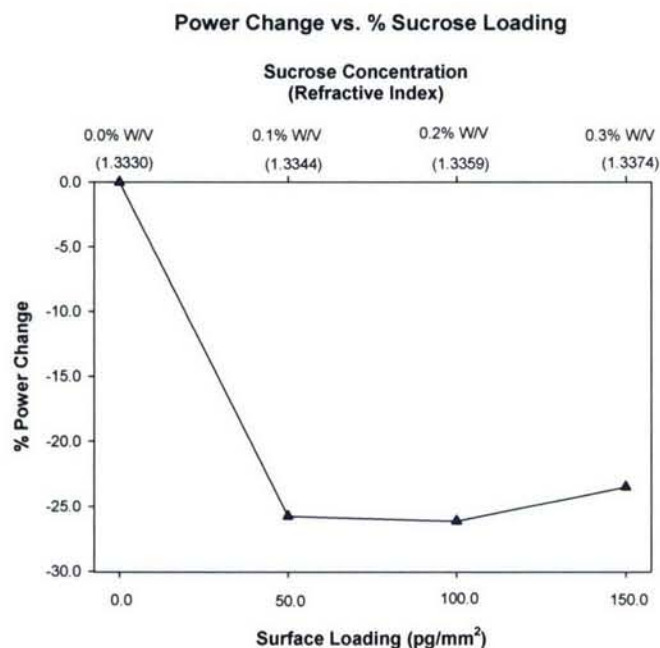


Fig. 9: SPARROW Transducer performance.

Biolayer Growth and Attachment

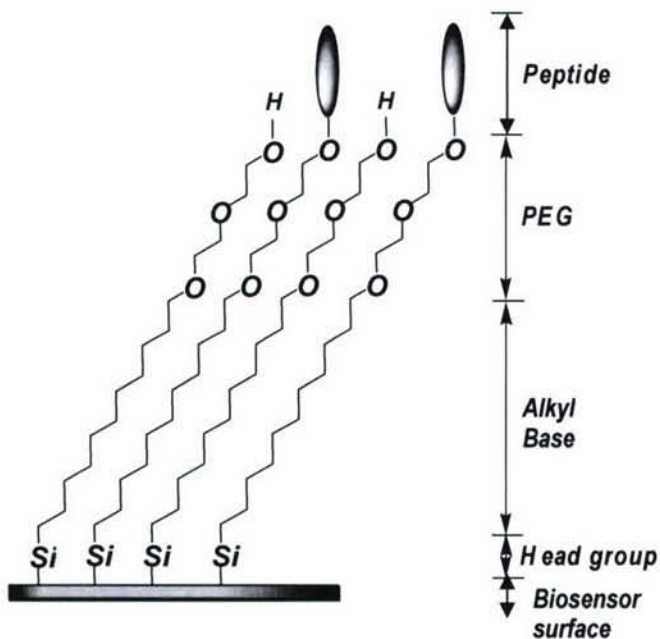


Fig. 10: Schematic of the biolayer system being developed. The self-assembled monolayer (SAM) monomers bind to the alumina surface through a silane surface and prevent binding of contaminant proteins and particles through the PEG groups (which are much longer in the real system). Some of the PEG groups are terminated with a peptide that corresponds to a signaling sequence that binds selectively to the surface of *B. subtilis* spores. The thickness of the entire biolayer is on the order of 5-nm.

derivatization schemes the molecules forming the coating do not stabilize each other the quality of the coating is highly dependent on the surface binding sites to have regular spacing at the appropriate distance. Most surfaces do not exhibit this level of homogeneity at the molecular level. Alumina is fairly rough at the molecular, compared with the gold surfaces SAMs are typically grown on. Thus, SAMs provide an excellent approach for creating even coatings, but challenges exist for coating rough surfaces and the efficacy of this strategy was not clear out the outset.

Ideally, the SAM monolayer should be very stable, but could be easily removed and regenerated after the exposure to the sample. Therefore, the formation and stability of the various SAM monolayers was studied initially. After it was determined that SAMs formed from monomers with carboxylic acid head groups were not stable enough in

For the SPARROW device to function properly, the surface must be coated with a thin homogenous layer that: i) minimizes non-specific binding and ii) selectively binds the target via molecular recognition. Our approach utilizes: self-assembled monolayers (SAMs) to provide a homogenous surface coating with minimal defects, terminal polyethylene glycol (PEG) tails to minimize non-specific protein adsorption, and a signaling peptide that selectively binds to a receptor on the target surface as shown in Figure 10.

SAMs were chosen to form the biolayer because they can form even, densely packed coatings, with minimal defects. During the SAM formation process the monomers interact strongly with each, which promotes binding, SAM stability, and complete coating. In direct

water, the use of monomers with alternate head groups of phosphonic acid and triethoxysilane was explored. Fundamental studies characterized the SAM formation on alumina and sapphire, and the stability of these SAMs in water solutions. The stability of the SAMs in water is crucial, because sample solutions containing the targets will be primarily aqueous solutions. SAMs formed from monomers with triethoxysilane head groups were found to be the most stable and were used in subsequent experiments.

A microfluidic channel was incorporated into the system to provide reproducible conditions for both reagent and target delivery, while minimizing the volume and mass of sample required. The binding and removal of target simulants were studied as a function of linear flow rate through the channel. In the working device, biohazards, such as anthrax, can be detected as spores, spore fragments, or individual proteins. Our approach focused on detection of whole spores, because it decreases the sample preparation needed. One micrometer diameter latex beads were first used as simulants for anthrax spores. The binding and removal of the beads was studied as a function of flow rate and surface morphology. Alumina and sapphire surfaces were studied as models for more heterogeneous and more homogeneous surfaces, respectively.

To determine if SAMs with minimal defects and high stability could be formed on aluminum oxide, the binding of an alkyl carboxylic acid, stearic acid (n-octadecanoic acid), was investigated. Under the appropriate conditions it was found that homogenous SAMs with minimal defects could be formed on atomically smooth aluminum oxide surfaces (sapphire at annealed at high temperature) with low surface defect density, and amorphous aluminum oxide surfaces (alumina) with high surface defect density [11]. The SAMs were characterized using primarily AFM, XPS, and DRIFT (diffuse reflectance infrared spectroscopy). Once it was determined that homogenous monolayers could be formed on sapphire and alumina, the stability of these SAMs in water was investigated. Water contact angles were used to measure changes in surface coverage upon exposure to water as shown in Figures 11 and 12. It was discovered that two regions of monomer binding to the surface exist: a region of rapid desorption and a region of slow desorption. These two regions provide evidence that the SAM monomers with carboxylic acid head groups bind to the atomically smooth terrace more weakly, which causes rapid desorption, while binding to the defect sites (steps, kinks, and atomic vacancies) is much stronger leading enhanced stability in these regions. In contrast, contact angles measured from SAM/alumina decrease monotonically without regional distinction because alumina contains different types of adsorption sites with various degrees of affinity. The interaction of the carboxylate head group with the aluminum oxide surfaces was investigated using DRIFT and XPS. It was found that the head group bound through mixed modes that vary from monodentate to bidentate. Differences in substrate interactions provide a range of SAM monomer binding energies. The monomers with lower binding energies have decreased stability and allow for the formation of pits in the SAMs. The AFM images of the desorption process are consistent with the loss of monomers from the SAM as evidenced by the formation of SAM islands. The AFM

images also show that the monomers desorb most rapidly from the terrace sites and bind more strongly at the step edges. These findings suggest that the substrate morphology plays a critical role in the SAM stability and must be carefully considered for non-permanent coatings. For this application, the alumina layers were deposited using chemical vapor deposition, to achieve the appropriate thickness on top of the silicon dioxide layer. Therefore, alterations of the alumina layer are not an option, and instead the biolayer or coating must be designed to compatible with these surface defects.

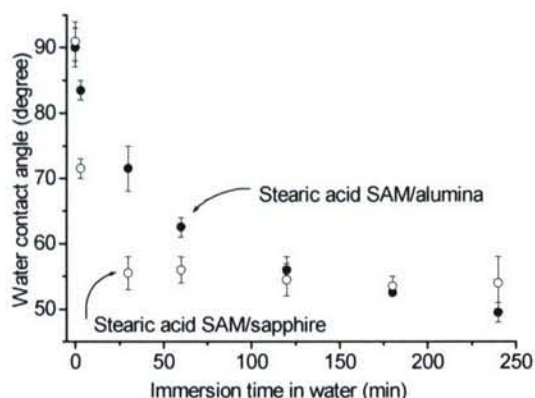


Fig 11: Water contact angles are used to measure the desorption of the SAM monomers. On sapphire, plotted contact angles are split into two regions: a region of rapid desorption and a region of slow desorption due to the crystalline nature of the underlying sapphire surface. In contrast on alumina, the contact angles decrease monotonically without regional distinction due to the amorphous nature of the underlying surface.

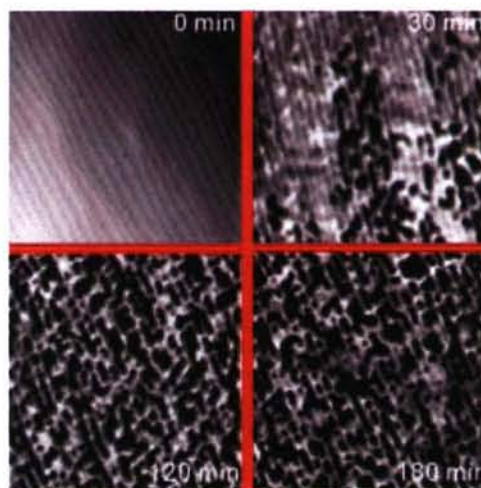


Fig 12: Figure 3. Tapping mode AFM images were obtained of SAMs of stearic acid after (a) 0 min (or fully covered SAM before immersion in water), (b) 30 min, (c) 120 min, and (d) 180 min of immersion in water. Stearic acid monomers self-assembled on the sapphire surface are progressively lost through molecular desorption into water.

The influence of anchoring groups of SAM monomers on the stability of a SAM in an aqueous environment was investigated for n-alkyl carboxylic acid ($-\text{CO}_2\text{H}$), n-alkyl phosphonic acid ($-\text{PO}_3\text{H}_2$), and n-alkyl silane ($-\text{SiCl}_3$), all of which have the same length of alkyl backbone chain. Each surface of the three SAMs was immersed in water for a designated time and its wettability was measured as shown in Figure 13. SAMs of alkyl carboxylic acid and alkyl phosphonic were found to desorb rapidly in water and are not stable enough for further biosensing applications. SAM monomers with triethoxysilane (TEOS) head groups were found to provide high surface coverage, and were very stable in water. The high stability of TEOS SAMs function well during initial detection events with the device, but unfortunately does not allow the surface to be regenerated. Regeneration of the surface in the device is challenging, because the SAM needs to be very stable during detection events, but must be easily altered after the detection event is completed. The TEOS SAMs do produce stable surfaces to minimize non-specific

adsorption and anchor the biomolecular recognition elements, and therefore provide a viable platform upon which a functioning biosensor sensor can be developed and characterized.

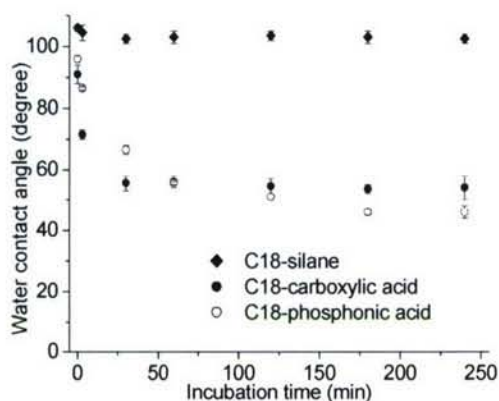


Fig. 13: A comparison of the stability of three SAM monomers with silane, carboxylic acid, and phosphonic acid head groups. Monomers with carboxylic and phosphonic acid head groups clearly create SAMs with much lower stability in water than the silanes. The silane SAMs are stable in water for months.

The next topic focused on was the microfluidic delivery of the spore simulants to the biosensor surface. Anthrax spores were simulated by using 1 μm latex beads. The latex beads bind non-specifically to the surface, providing significant coverage with which to access the detection limits and further develop the microfluidic system and methods. The first objective addressed was to determine the effect of flow rate of bead binding and removal. It is important to note the beads or spores are very large compared to molecules, and the hydrodynamic forces on the microbeads are significant. Furthermore, it is anticipated that the optimal flow rates for adsorption and desorption will be dependent on the

bead or target size, because the flow velocity profile across the channel height is parabolic with the flow rate at the wall equal to zero. We have shown that the 1- μm beads can be attached at a linear flow rate of 2.7 mm/min. Following attachment of the beads, their detachment behavior was monitored by flowing a blank solution over the bead-attached surface and increasing the flow rate from 4.4 to 89 mm/min in increments of 4.4 mm/min. The flow rate used during loading is critical because exceeding the desorption limit during loading, would obviously prevent detection. The loading flow rate also determines the time that it takes to process a sample, and is a key parameter for the determination of the limits of detection. The effect of surface morphology on the microbead adsorption and desorption was investigated by comparing the adsorption and desorption of the beads on two surfaces: alumina and sapphire. The sapphire surface was smooth at the atomic level and represented a more homogenous surface. It was found that with the more homogenous sapphire surface the microbeads desorbed over a more narrow range of linear flow rates as shown in Figure 14. These results suggest that more homogeneous surfaces provide a narrower range of binding strengths to the surface, and a narrower range of flow rates for adsorption and desorption. The peak in microbead removal as a function of flow rate may provide an additional feature for identification in a manner similar to a retention time in chromatography. These preliminary results are promising and suggest that greater selectivity can be achieved with the more homogeneous PEG-peptide layer that we are developing. Currently, it is not clear if real

spores can be removed from the sensor surface by simply increasing the flow rate. Future studies will be required to determine if the non-covalent interactions between the spore and biomolecular recognition element can be broken while leaving the biomolecular recognition element intact. Similar studies using 200-nm latex beads have been initiated, but not completed. The smaller beads serve as a model for smaller spores or spore fragments.

The first steps have been made towards utilizing spores of *B. subtilis* as an anthrax simulant. *B. subtilis* have been fluorescently labeled and desorbed nonspecifically on the biosensor surface as shown in Figure 15. Although binding is non-specific this work will provide estimates for the lowest percent surface coverage that can be detected. When combined with the flow rate data a detection limit, in the form of a concentration, can be determined. This information will be a great step forward in determining the useful working range of a completed device.

Much important proof of concept work has been achieved including coating of the surface with PEG terminated SAMs and application of the stimulant beads through the microfluidic channel. However, a number of important achievements must still be made. First a biomolecular recognition element, such as a signaling peptide or antibody must be attached to the surface. For this purpose, a peptide with the sequence NHFLPKVG, which binds selectively to the surface of anthrax stimulant, *B. subtilis*, [12,13,14] will be coupled to the end of a PEG SAM monomer to provide a surface that will selectively bind a target spore. We have the both the PEG SAM monomer and the peptide with blocked functional groups, but still need to couple them. Once the molecules are coupled they will be used to coat the sensor surface to test for the selective binding of *B. subtilis*. Once selective binding is achieved, the flowrate studies will be reproduced to provide this important data for a real biomolecular system. When this surface is produced it will be tested with the simulant to determine the limits of detection and the selectivity of the device. These two figures of merit are critical for establishing its utility as a sensor.

Another important area for future work is the regeneration of the surface. From our work with the SAM monomers with carboxylic and phosphonic acid head groups, it appears that formation of a stable SAM is a signal step that can be regenerated is unlikely. In short, increasing the stability of the SAM makes it more difficult to regenerate, and decreasing the stability, while making it easier to regenerate, decreases stability.

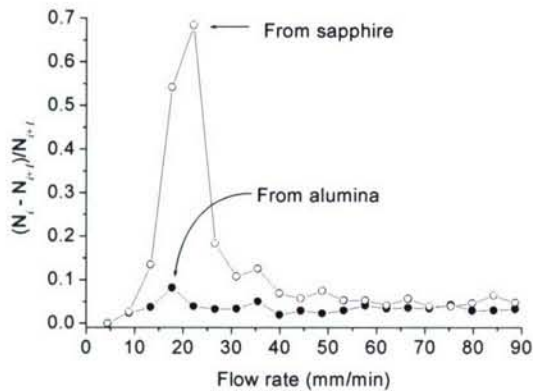


Fig. 14: (left) The desorption of 1-mm latex beads from the surface of alumina and sapphire. The beads gradually desorb from the amorphous alumina surface over a wide flow rate range. In contrast, desorption is nearly complete and occurs over a narrow range (as indicated by the peak) from the more homogeneous sapphire surface. These results indicate that more homogeneous surfaces provide narrower adsorption and desorption ranges. Additionally, it may be possible to remove the spores from the surface by simply increasing the flow rate.



Fig. 15: (left) Fluorescently labeled *B. subtilis* spores nonspecifically adsorbed on an alumina waveguide surface.

An excellent approach for the SAM, is to incorporate a functional linker into the SAM monomers that can be specifically cleaved by using a specific reagent, photoactivation, or application of a potential. For instance and ω unsaturated ester can be converted photochemically to a lactone, cleaving part of the molecule (which would be the PEG peptide in our case). The lactone can be converted back to the ω unsaturated ester through a nucleophilic addition. An exciting aspect of using photocleavage is that the light for photocleavage can be supplied using the top waveguide. Use of the waveguide provides a means to direct modification and regeneration of the sensor surface only. Modification of the microchannel walls outside of the region of detection can thus be prevented. This renewable surface chemistry will have broad applicability and be useful for numerous applications. Surface regeneration is required to improve the useful lifetime of biosensors, because even the best coatings foul eventually. Additionally, a straightforward means is provided for simultaneous regeneration of the molecular recognition elements. This synthesis and characterization of a stable coating that can be regenerated could be the subject of future work.

Theoretically Obtainable LOD for SPARROW and Similar Devices

The anticipated theoretical limit of detection (LOD) of the SPARROW device and similar coupled waveguide architectures is now addressed.

Biosensors based on coupled or resonant optical waveguides have been reported in recent years [e.g. 15,16]. By monitoring changes in the output power of the waveguides, these biosensors can detect binding events of specific targets selectively bound to biolayers at one or more of their waveguide surfaces. The Stacked Planar Affinity

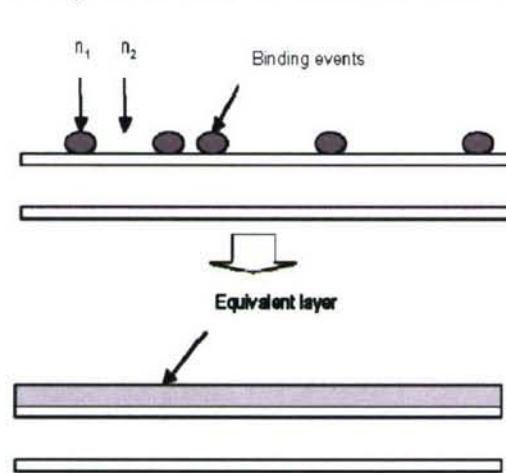


Figure 16: Depiction of target binding equivalent layer on stacked waveguides (white rectangles).

Regulated Resonant Optical Waveguide (SPARROW) device uses a stacked planar waveguide architecture with the biolayer on the topmost guide in aqueous analyte contact. To determine the theoretical Limit of Detection (LOD) of the SPARROW or other resonant waveguide-based biosensor, the influence of the sparse, random spatial distribution of target binding events indicative of low surface loadings of application interest (pg/mm² or less) must be determined. This random distribution of targets on the biolayer and waveguide surface will result in both scattering loss and a change in the coupling condition resulting in detuning of the resonant waveguides. These physical effects each result in a change to the output power from the

device. While several mathematical models for coupled waveguides have been established with which some non-ideal conditions such as surface roughness have been addressed [17,18,19], consideration of this problem has not been addressed. We provide an analytic model that uses both coupled waveguide theory and the Volume Current Method (VCM) to capture the coupling and the scattering behavior of surface loaded waveguides common in resonant waveguide biosensors.²⁰ The analytic model is used to numerically determine the theoretical LOD for a SPARROW device as a function of target size and optical sensitivity. The methodology is broadly extendable to other device geometries relying on resonant waveguide detuning arising from selective biotarget attachment.

Generally, coupled waveguide-based optical biosensors sense target binding due to the effective change this binding creates in refractive index of the cladding region of one waveguide. Once targets bind within the biolayer on this waveguide, the propagation constant of this waveguide will change while that of the other waveguide remains effectively the same, changing the coupling condition between the two waveguides. Therefore, the monitored output power at the end of the waveguides could either increase or decrease. Setting the refractive index of cladding and binding events as n_1 and n_2 and the surface coverage as κ , we use an equivalent layer to replace this random binding region (Fig. 16). The height of the layer is equal to the height of the target binding events. The refractive index of the equivalent layer n_{eq} is expressed as

$$n_{eq} = [n_2^2 * \kappa + n_1^2 * (1 - \kappa)]^{1/2} \quad (1)$$

Here, n_{eq} must be constrained to be less than the effective refractive index of the top waveguide to satisfy the requirements of further derivations. The new propagation constant in this waveguide can now be calculated and the change of output power predicted.

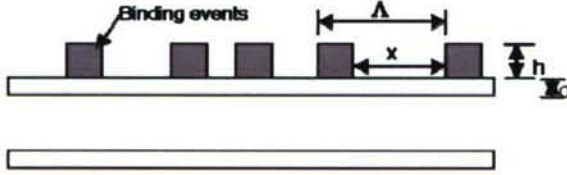


Fig. 17: Binding event simulation on the waveguide surface.

Random binding events will result in scattering loss and a reduction in output power. Since the binding is totally random, we consider that the distance between each two adjacent binding events (referred to here as interparticle distance) follows the normal distribution function

$$P(x) = \exp[-(x - \mu)^2 / 2\sigma^2] / \sigma / (2\pi)^{1/2} \quad (2)$$

where σ is the standard deviation and μ is the average interparticle distance which depends on the surface coverage. Once $S(x)$, the relationship between the scattering loss and the interparticle distance, is known, the total scattering loss at low surface coverage can be approximated as

$$F = \int (N - 1) P(x) S(x) dx \quad (3)$$

where, N is the number of total binding events and is assumed small. The integrating region extends over the length of the waveguide with target surface coverage

$$L_{max} = L_{waveguide} (1 - \kappa) \quad (4)$$

To simplify the calculation of $S(x)$, we simulate the binding events as rectangular particles (Fig. 17). In the low surface coverage condition of interest, the scattering loss should be small so that the volume current method (VCM) can be used [19]. For the TE single mode waveguide, the scattering loss fraction $S(x)$ is derived as

$$S(x) = [(\epsilon_1 - \epsilon_2)^2 k^2] / \{4\epsilon_1\epsilon_2\Lambda h[1 + \exp(\alpha h) / \alpha h]\} \times \int_0^\pi |A|^2 |E|^2 |D|^2 d\theta \quad (5)$$

where

$$A = 1 + \exp[i\Lambda(\beta - k \sin \theta)] \quad E = \int_0^h \exp[iz'(\beta - k \sin \theta)] dz' \quad D = \int_0^{h+d} \exp(-ikx' \cos \theta) dx' \quad (6)$$

k is the wavevector, β is the propagation constant, and ϵ_1 and ϵ_2 are the permittivity of the binding events and cladding region, respectively. Other parameters are defined in Fig. 17.

For a certain surface coverage such as κ , the change of output power can be expressed as

$$\Delta P(x) = \Delta P_c(x) + S(x), \quad (7)$$

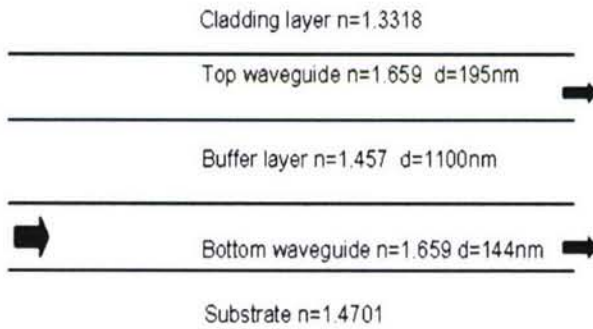


Fig 18: An example SPARROW transducer structure. Incident beam is input to the bottom waveguide. Wavelength of incident beam: 632.8nm. Length of waveguide interaction 743.11mm

where ΔP_c is the change of output power arising from the change of coupling condition and S is the scattering loss from randomly distributed binding events. Notice that S is always negative (reducing power) and ΔP_c could be either negative or positive. With correct choice of device operating point, $|\Delta P(x)|$ will be larger when both ΔP_c and S are negative resulting in higher device sensitivity. If the minimum detectable percent change in optical power is ΔP_m , for binding event detection we require

$$|\Delta P(x)| \geq \Delta P_m \quad (8)$$

At a particular surface coverage κ_s , $\Delta P(x_s) = \Delta P_m$. Once this particular coverage and the mass density of binding events are known, the LOD can be easily calculated.

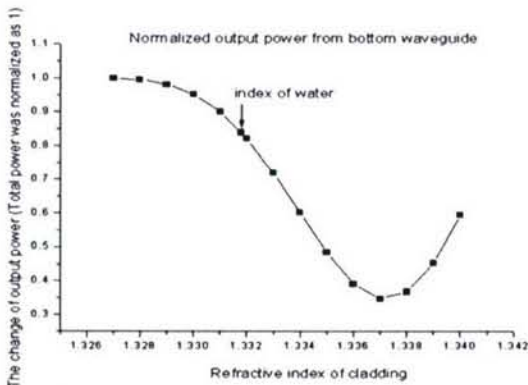


Fig 19: SPARROW bottom waveguide output power as a function of cladding index.

Fig. 18 gives an example SPARROW structure supporting TE mode propagation. Since this device is operated in a water environment, the cladding index before binding will be equal to the index of water (1.3318). If monitoring the output power from the bottom waveguide, we would find the change of output power as a function of cladding index shown in Fig. 19. Usually, the refractive index of binding events which we use (1.4 – 1.5) is larger than that of water. Thus, the effective index of the cladding will increase after binding resulting in the reduction of output power

(see Fig. 19). Assuming the mass density of these binding events is 0.081 g/mL (mass density of anthrax spores), an interaction length is 743 μm (four times the coupling length), the size of binding events is 200 nm and their index is 1.5, we obtain the relationship between the change of output power and the surface coverage shown in Fig. 20. In this case, if the minimum detectable percent change in optical power is 0.1%, we find the corresponding surface coverage is 0.0625%. Therefore, the LOD for such binding events will be 0.21 pg/mm^2 . However, if the size of bound targets changes to 40nm, the LOD will be 0.41 pg/mm^2 . Fig. 21 shows the different LOD for different target sizes and different minimum detectable percent change in optical power.

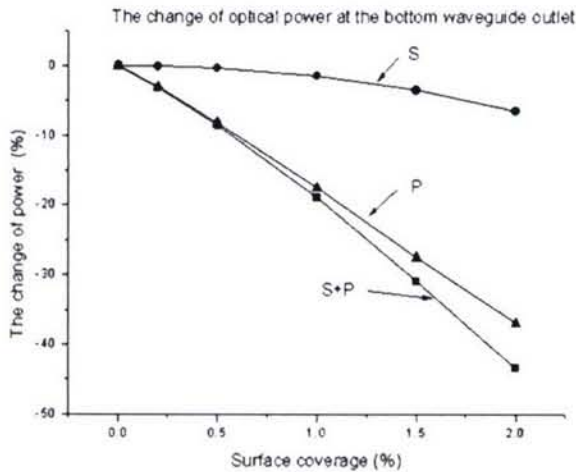


Fig 20: The relationship between surface coverage and the change of output power

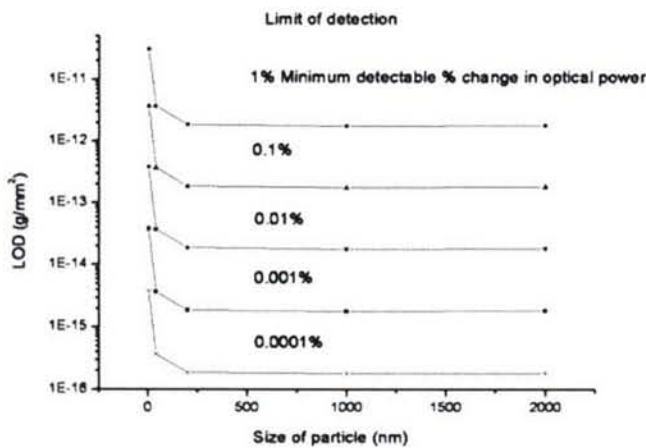


Fig 21: The LOD as a function of bound target size for different minimum detectable change in optical power.

In summary, we have developed a methodology to numerically determine the theoretical LOD for biosensors based on coupled waveguides under the condition of small, spatially random surface loading. The approach treats the contribution of both optical scattering due to target binding and resonant waveguide coupling to the LOD. The technique was applied to the SPARROW biosensor for the case of TE mode propagation and targets taller than the evanescent field penetration depth. However the approach can be broadly extended to other device geometries relying on resonant waveguide detuning arising from selective target surface binding. Important future work would include adapting this basic model to predict the LOD performance of this class of devices for smaller targets.

Impact on Research and Education Infrastructure

This award has had a tremendous impact on the infrastructure supporting interdisciplinary scientific discovery at WVU. This project was the nucleation point of efforts at the university at the bio-nano interface linking the engineering, physical and health sciences. This was the first project which served as a model for others in their efforts to build and grow collaborations across the physical, health, and engineering sciences in the area of molecular recognition and detection. The group that executed this work was the first of a cohort of interdisciplinary groups that now form the *WVNano Initiative* exploring this area among others. This initiative, begun in 2004 soon after award of this grant, is now a statewide effort which has received a \$9M NSF Research Infrastructure Initiative Award and matching state and university support. The WVNano Initiative web site is <http://wvnano.wvu.edu>.

This research continues to result in the interdisciplinary training of a cohort graduate students and undergraduate students.

Postdoctoral Associates:

Chemistry: 1

Graduate Assistants:

Chemistry PhD: 1

EE Masters: 3

EE PhD: 1

Undergraduate Student Researchers:

Chemistry: 1

Engineering: 3

The interdisciplinary undergraduate research training approach that in part resulted from this project contributed to the recent award of an NSF Nanoscale Undergraduate Education Award, one of ten made nationally, to establish an undergraduate *Nanosystems Emphasis*. This ONR funded work was among the core projects that resulted in an NSF REU Site Award received by WVNano in 2007. The project engaged two undergraduates in the 2007 summer program.

References

1. Prasad and A. N. Chandorkar, J. Appl. Phys., 94, 2308 (2003)
2. T. Cornell, J. R. Nightingale, S. Pathak, L. A. Hornak, and D. Korakakis, "Thickness and Fourier transform infrared peak instability in silicon dioxide thin films deposited using electron-gun deposition," Journal of Vacuum Science and Technology B," 24 (5), 2250 (2006)
3. Prasad and A. N. Chandorkar, J. Appl. Phys. 94, 2308 (2003)
4. K. H. Guenther, "Microstructure of vapor-deposited optical coatings," Applied Optics, 23 (21), 3806 (1984)
5. P. Martin, R. P. Netterfield, and W. G. Sainty, "Modification of the Optical and Structural Properties of Dielectric ZrO₂ Films by Ion-Assisted Deposition," J. Appl. Phys., 55, 235 (1983).
66 P. J. Martin, "Ion-beam-assisted deposition of thin films," Applied Optics, 22 (1), 178 (1983)
7. R. Ulrich and R. Torge, "Measurement of Thin Film Parameters with a Prism Coupler," Applied Optics, 12(12), 2901 (1973)
8. P. Poloju, P. Samudrala, J. R. Nightingale, D. Korakakis, and L. A. Hornak, "Characterization of Alumina Optical Waveguides Grown by Ion Beam Assisted Deposition for SPARROW Biosensors," MRS Fall 2006 Conference Proceedings
9. Samudrala, P. "Optical Characterization of Alumina Waveguides and SPARROW Biosensor Modeling," Master's Thesis, West Virginia University (2006)
10. J. R. Nightingale, T. Cornell, P. Samudrala, P. Poloju, L. A. Hornak, D. Korakakis, "Reactive Deposition of Dielectrics by Ion Beam Assisted E-beam Evaporation," MRS Fall 2006 Conference Proceedings
11. M. S. Lim, K. Feng, X. Chen, N. Wu, A. Raman, E. S. Gawalt, J. Nightingale, D. Korakakis, L. A. Hornak, and Aaron Timperman, "Adsorption and Desorption of Stearic Acid Self-assembled Monolayer on Aluminum Oxide," Langmuir, 23 (5) pp 2444 – 2452 February 27, 2007
12. Knurr, J.; Benedek, O.; Heslop, J.; Vinson, R. B.; Boydston, J. A.; McAndrew, J.; Kearney, J. F.; Turnbough, C. L., Jr. *Peptide ligands that bind selectively to spores of Bacillus subtilis and closely related species*, Applied and Environmental Microbiology **2003**, 69, 6841-6847.
13. Turnbough, C. L. *Discovery of phage display peptide ligands for species-specific detection of Bacillus spores*, Journal of Microbiological Methods **2003**, 53, 263-271.
14. Williams, D. D.; Benedek, O.; Turnbough, C. L., Jr. *Species-specific peptide ligands for the detection of Bacillus anthracis spores*, Applied and Environmental Microbiology **2003**, 69, 6288-6293.

15. D. Lloyd, L. A. Hornak, S. Pathak, D Morton, and I. Stevenson, "Application of Ion Beam Assisted Thin Film Deposition Techniques to the Fabrication of a Biosensor Chip with Fieldability Potential for Important Biohazard Detection Applications," in Proceedings of 47th Annual Technical Conference, Society of Vacuum Coaters 505/856-7188. p334-339 (2004)
16. Luff, B. J., Harris, R. D., Wilkinson, J. S., Wilson, R. and Schiffrin, D. J., "Integrated optical directional coupler biosensor," *Opt. Lett.* 21 (8) , p618-620 (1996)
17. Huang, W., "Coupled mode theory for optical waveguides: an overview," *Opt. Soc. Am. A.* 11(8) p963-983 (1994)
18. Ladouceur, F., "Roughness, Inhomogeneity, and Integrated Optics." *Journal of Lightwave Technology.* 15(6) p1020-1025 (1997)
19. Garcia-martin A. Saenz, J.J., "Statistical properties of wave transport through surface-disordered waveguides." *Waves in random and complex media,* 15(2) p229-268, (2005)
20. K. Feng and L. A. Hornak, "Theoretical Limit of Detection of Coupled Waveguide – Based Biosensors," submitted to *Applied Optics.*